Evaluation of Neutron Light Output Response Functions in EJ-309 Organic Scintillators

Mark A. Norsworthy[a,*], AlexisPoitrasson-Rivière[a], Marc L. Ruch[a], Shaun D. Clarke[a], Sara A. Pozzi[a]

[a] Department of Nuclear Engineering and Radiological Sciences, University of Michigan, 2355 Bonisteel Blvd, Ann Arbor, MI 48109, USA
* Corresponding author. Tel.: +1 734 250 9235; Fax: +1 734 763 4540

E-mail addresses: marknors@umich.edu (M.A. Norsworthy), alexispr@umich.edu (A. Poitrasson-Rivière), mruch@umich.edu (M. L. Ruch), clarkesd@umich.edu (S. D. Clarke), pozzisa@umich.edu (S. A. Pozzi).

KEYWORDS

Organic scintillator, light output, neutron detection, quenching, MCNPX-PoliMi, detector characterization

AUTHORS

M. A. Norsworthy, A. Poitrasson-Rivière, M. L. Ruch, S. D. Clarke, S. A. Pozzi

ABSTRACT

An accurate model of the nonlinear detector response of organic scintillators to neutrons is required to correctly simulate fast neutron detection, as well as interpret measured pulse height data. Several empirical and semi-empirical models are available to fit measured scintillator light output data. In this work, EJ-309 light output data from neutrons depositing 1.15 MeV to 5.15 MeV on hydrogen wereanalyzed using empirical models as well as semi-empirical models based on the work of Birks and Voltz. Although all tested models fit the experimental light output data well in the measured range, the models were observed to diverge in low-energy extrapolation. The modelswerethen tested by comparing a measurement and MCNPX-PoliMi simulation of an EJ-309 detector response to fast neutrons from a ^{252}Cf spontaneous fission source. The agreement between the measured and simulated pulse height distributionsvaried significantly depending on the light output model used. The best agreement between simulated and measured neutron pulse height distributionswas achieved by using the Birks model. The bin-by-bin agreement was better than 5% over the range 0.08 to 2.18 MeVee, and better than 10% from 2.18 to 3.13 MeVee. The integral count rate over the range 0.08 to 3.14 MeVee differed by less than 1% in absolute units.

1.0 Introduction

The IAEA is interested in high-fidelity Monte Carlo modeling of detector technologies for international safeguards applications[1]. Several ongoingsafeguards projects employ organic scintillators as fast neutron detectors, such as theLiquid-Scintillator Neutron Coincidence Collar (LS-NCC) [1],the Fast Neutron Multiplicity Counter (UM-FNMC) [2,3],radiation portal monitors (RPMs)[4,5], and the Dual Particle Imager (DPI) [6–8]. Organic scintillators are also frequently employed in a wide variety of applications including, but not limited to, nuclear physics [9], material characterization [6,3,10,2], imaging [6–8], and nuclear medicine[11,12].

In organic scintillators, interactions with hydrogen produce the majority of the neutron-induced scintillation light; the amount of light produced is a nonlinear function of the energy deposited. The light output function affects every neutron event in both Monte Carlo simulations and the interpretation of experimental data. In experiments, it is used to convert collected light (proportional to pulse height) to energy deposited, which is a key parameter in neutron spectroscopy and imaging applications. In Monte Carlo simulations, the energy deposited by each neutron interaction is known, and the light output function is used to simulate pulse heights. More accurate light output functions would yield more accurate simulations of detector response, more reliable simulated neutron efficiency, and improve the results obtained when using simulated response matrices for spectrum unfolding. Ultimately, these improvements would benefit the design of detection systems for inspections, treaty verification activities, nuclear material accountancy, and other safeguards programs.

Careful measurements are required to generate the light output function. These measurements usually result in a discrete set of data points relating energy deposition to light output. To fill in gaps between data points, as well as to extrapolate to lower and higher energies, these data are fitted using a variety of functional formsranging from simple polynomials[13],rationals of polynomials[13],power laws[14],and exponential functions[13,15] tosemi-empirical models such as those proposed by Birks and Voltz [16–19].

This paper demonstrates that the choice of functional form for the light output function for neutron interactions on hydrogen profoundly impacts the accuracy of simulated pulse height distributions (PHDs). The choice of neutron light output function also alters the calculation of neutron detection energy thresholds, and has direct consequences on neutron unfolding, dosimetry, and imagingresults. In particular, this paper concerns the divergence of the various light output models in extrapolation to low energies, and the corresponding effect on simulated pulse height distributions.

We revisit the EJ-309 light output data of Enqvistand colleagues[13] and fit them to various functional forms. We show that many forms can be chosen that give good fits to the measured light output data points, but they diverge significantly from one another in extrapolation. We then use the code MCNPX-PoliMi [20]to simulate EJ-309 detector response to neutrons from a ^{252}Cf spontaneous fission source, and we use the post-processing code MPPost [21]to apply the different light output functions to generateneutron PHDs. We compare the simulated PHDs to measured data and conclude that the semi-empirical functional forms perform significantly better than the commonly used empirical forms.

2.0 Background

Kornilovand colleagues[22]showed that a rational function of polynomials could give a good fit for a quick estimate, but for calculations demanding higher degrees of accuracy, more complex equations were required. Kornilovand colleagues[22]and Enqvistand colleagues[13]made use of an exponential functional form. The formeralso explored one of the semi-empirical functional forms, based on Birks' Law, achieving better agreement with experimental data. All of these forms are tested in this work, in addition to a relationship proposed by Voltz and colleagues[17–19]. Table 1 shows all of the functional forms that are examined in this work, where E is the neutron energy deposited on hydrogen, and L is the light produced in the scintillator. The coefficients a, b, c are computed in the fits.

Table 1. Neutron light output equations tested in this work.

"Polynomial"	$L(E) = aE^2 + bE + c$	(1)
"Rational"	$L(E) = \frac{aE^2}{E + b}$	(2)
"Power Law"	$L(E) = aE^b$	(3)
"Exponential"	$L(E) = aE - b\left[1 - \exp\left(-cE^d\right)\right]$	(4)
"Birks"	$L(E) = \int \frac{a}{1 + b(\frac{dE}{dx})} dE$	(5)
"Voltz"	$L(E) = a \int \left[(1-c) \exp\left[-\frac{b(1-c)dE}{dx}\right] + c\right] dE$	(6)

The two semi-empirical functions are based on the concept of ionization quenching: a reduction in the amount of light produced versus that which would be produced by a gamma ray depositing equal energyto a recoil electron. In both models, quenching increases with increasing ionization density, which in turn increases with stopping power (dE/dx). Fig. 1 shows the stopping power of protons and electrons in EJ-309, as determined by the use of the SRIM software package [23,24] and the NIST ESTAR database [25], respectively. These are the stopping power values used throughout this work.

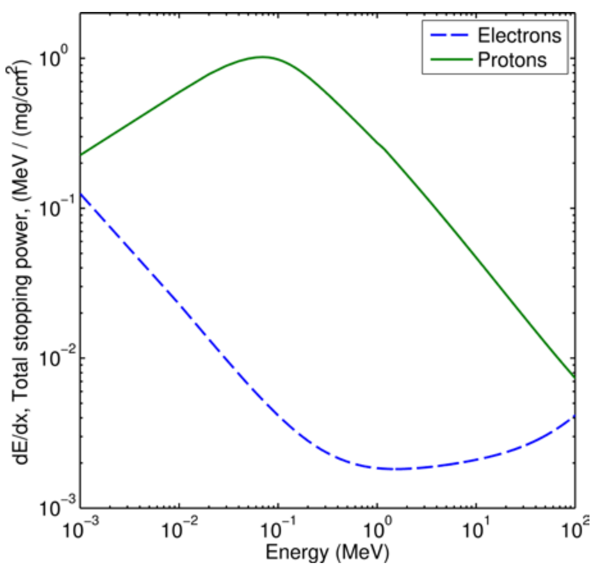

Fig. 1. Total stopping power of electrons and protons in EJ-309 liquid scintillator, generated using the NIST ESTAR database [25] and the SRIM-2012 package[23,24], respectively .

The forms used in this work for Birks' Law (Eq. 5) and Voltz' equation (Eq. 6) are the integrals over energy of Eq. 3 and Eq. 6 in Brooks and colleagues' review paper[17]. Because our work is far from relativistic energies, we introduce an approximation of Voltz' model in which F_s(c in Eq. 6) is fitted as a constant instead of a function of charge and energy as in Ahlen and colleagues[19].

3.0 Light Output Fitting Methodology

We reconstructed light outputdata points as a function of energydeposited, *L(E)*,from a time-of flight measurement performed at the Edwards Accelerator Facility at Ohio University [13]. The measurement was performed witha 12.7 cm thick x 12.7 cm diameter EJ-309 liquid scintillator detector coupled to a Photonics XP4512B photomultiplier tubes (PMT).The data were generated using a 10-meter flight path and neutrons were generated using the ^{27}Al(d,n) reaction resulting in a white source containing a wide range of energies. Time-of-flight was used to sort neutrons with energies from 1.15 to 5.15 MeV in 100 keV-wide bins. Because neutrons can deposit any fraction of their energy in each collision on hydrogen, it can be difficult to determine the pulse height corresponding to a single full-energy transfer; however, as will be seen later in this work, the light output function is concave in this energy range, meaning that a single scatter yields more light than any two smaller scatters depositing the same total energy. Following Kornilov[22], the binned PHDs were smoothed, differentiated, and a Gaussian was fitted to the rightmost peak ofthe derivative. The mean of the Gaussian was taken as the pulse height corresponding to a neutron scattering once on hydrogen and depositing all of its energy.

It should be noted that in this work, as in[13], the term ‘pulse height’ refers to the maximum of the digitized pulse, as opposed to the pulse integral. Pulse height is not always proportional to pulse integral, so it is not in general possible to easily translate between pulse height and pulse integral based light output functions. However, although the absolute values will vary, the methodology used here would also be applicable to pulse integral data.

Generation of the empirical fits was performed using the MATLAB Curve Fitting Toolbox[26]. Enqvistand colleagues fixed the exponent to 1.0, as did Takada[13,27]. Byrd and Urban[14] cite Madey[28], who determined an exponent of 0.9. To explore the range of behaviors associated with different exponents when using the exponential functional form (Eq.4), the variable*d* was fixed to discrete values ranging from 0.9 to 1.1.

In order to fit coefficients for the semi-empirical models, the integrals in Eqs. 5 and 6 were evaluated numerically using the trapezoidal rule.The resulting sets of ordered pairsof energy and light output could then be interpolated to determine the light output (MeVee) corresponding to the measured data points’ energy(MeV) values. The curve fitting toolbox was used to vary the coefficients and compare thelight outputto the measured values using a nonlinear least squares algorithm.

All of the fitted light output equationsare displayed in Table 2; a subset of the fits is displayed in Fig.2. The fit from Enqvistand colleagues[13] is shown for reference.

Table 2.12.7 cm thick x 12.7 cm diameter EJ-309 detector neutron light output modelcoefficients and goodness of fit values. Italics indicate coefficients that were fixed during the fitting process.

Form	a	b	c	d	SSE	R^2	RMSE	ID
Exponential	*0.748*	2.41	*0.298*	*1.000*	0.0037	0.9998	0.0096	Exponential1*
	0.944	6.25	0.144	*0.900*	0.0028	0.9998	0.0087	Exponential2
	0.782	2.98	0.251	*0.950*	0.0024	0.9998	0.0080	Exponential3
	0.634	1.45	0.427	*1.050*	0.0028	0.9998	0.0086	Exponential4
	0.605	1.24	0.477	*1.100*	0.0031	0.9997	0.0091	Exponential5
Rational	0.7836	5.523			0.0026	0.9998	0.0082	Rational6
Polynomial	0.03937	0.2062	-0.1454		0.0031	0.9997	0.0090	Polynomial7
Birks	2.277	33.84			0.0062	0.9995	0.0126	Birks8
	1	11.12			0.0635	0.9947	0.0398	Birks9
Voltz	0.9134	6.854	0.07178		0.0026	0.9998	0.0083	Voltz10

	1	8.345	0.09375		0.0033	0.9997	0.0093	Voltz11
Power Law	0.1387	1.618			0.0055	0.9995	0.0119	Power**

* Fit from [13].
**Power Law fit was not used during post-processing using MPPost of MCNPX-PoliMi simulations.

From examination of Table 2, it is apparent that most of the modelsgive “good” fits to the data points (high R^2, low SSE). It would be difficult to choose the best parameterization in a non-arbitrary way based on these metrics.Fig.2shows the measured light output data and six of the models on a log-log scale covering proton recoil energies from 10 keV to 7 MeV. It is clear that different modelsshown diverge significantly from one another, especially at low energy, while they all fit the measured data points well.

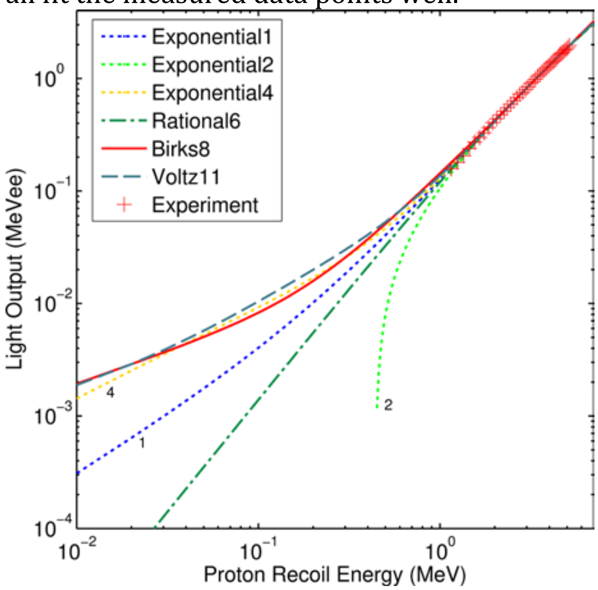

Fig. 2. Log-log plot showing the measured light output data points for the 12.7 cm thick by 12.7 cm diameter EJ-309 detector as well as a subset of thevarious fits extrapolated from 0.01 to 7 MeV proton recoil energy.For legibility, not all fits tested are plotted. The fits shown were selected to illustrate the divergent behavior at low energy.

Further, the extrapolations of the exponential functional form are sensitive to the valueof variable*d*. The later sections of this paper show that an exponent greater than 1 is required to give the best results at low energies; a possible explanation for this based on the behavior of the proton stopping power will be discussed in Section 5.0.

In light of the manyoptions available, choosing a model is challenging. An independent way to test and validate, or at least inform, the choice of modelis required. The nonlinear nature of the light output requires consideration of each individual neutron scatter event in the detector. For our work we used the Monte Carlo code, MCNPX-PoliMi [20]. Each energy deposition was converted to light using an enhanced version of the post-processing code MPPost [21] that allows the use of the Birks and Voltz models.

4.0Validation Measurement Methodology

In order to test light output coefficients, a validation measurement using a well-known source was conducted as a baseline. Wemeasuredspontaneous fission neutrons from a recently manufactured ^{252}Cf source, calibrated by the vendor with a 5% tolerance. At the time of the measurement, the source strength was calculated to be 5.44 mCi, with aspontaneous fission rate of 6.23×10^6 fissions/s and a corresponding neutron emission rate of 2.34×10^7 neutrons/s. The uncertainty on these values is estimated to be 5%.

The same 12.7cm thick x 12.7 cm diameter cylindrical EJ-309 liquid detector coupled to a Photonics XP4512B PMT that was used for the *L(E)* measurement was used to measure the ^{252}Cf source. The detector was placed at a distance of 116.4cm from the source. A 7.62cm thick x 7.62cm diameter cylindrical EJ-309 liquid detector coupled to a ET-Enterprises 9821B PMT was also used and placed 112.7cm from the source.

The voltage output was measured from the anode of the PMT and digitized using a CAEN DT5720 12-bit 250-MHz waveform digitizer. Neutron and photon pulses were discriminated using the charge-integration method[29], in which the integrals of two different time windows corresponding to the "tail" and the "total" pulse are compared. Fig.3shows a log-scale histogram of a subset of the measured data plotted with the tail integral versus the total integral. The upper distribution means the pulse had a larger "tail" component than in the lower distribution, so the upper distribution corresponds to neutron pulses and the lower corresponds to photon pulses. For this work we utilized the software tool,SlicePSD[30] to generate the discrimination line in a robust and repeatable way. The SlicePSD generated discrimination line is displayed as the red line on Fig.3.

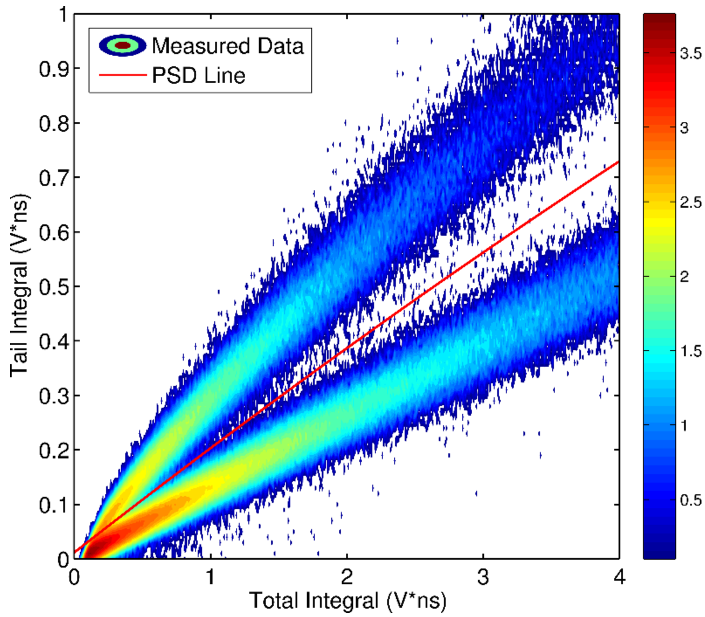

Fig.3. Log$_{10}$ scale histogram of ^{252}Cf pulses measured using the 12.7 cm thick x 12.7 cm diameter EJ-309 detector. The ordinate shows the integral of the "tail" of the pulses, while the abscissa shows the "total" integral of the pulses. The upper band corresponds to neutron pulses while the lower band corresponds to photon pulses. The discrimination line is shown in red.

The lower threshold was set to 0.02 V, which corresponded to approximately 32 keVee. The upper threshold was approximately 3.15 MeVee, due to the 2-V dynamic range of the digitizer.

The measured neutron PHD is shown in Fig.4. The error bars shown are from counting statistics, corresponding to one standard deviation. The peak in the distribution is at ~0.08 MeVee – below that pulse height, particle misclassification is more prevalent. The pulse shape discrimination (PSD) line was chosen to capture as many true neutrons as possible while avoiding the densest part of the gamma ray distribution to avoid excessive gamma ray misclassification (false positive neutrons). This line results in reduced neutron efficiency in this pulse height region, but greater confidence that the pulses selected were true neutrons rather than misclassified gamma rays.

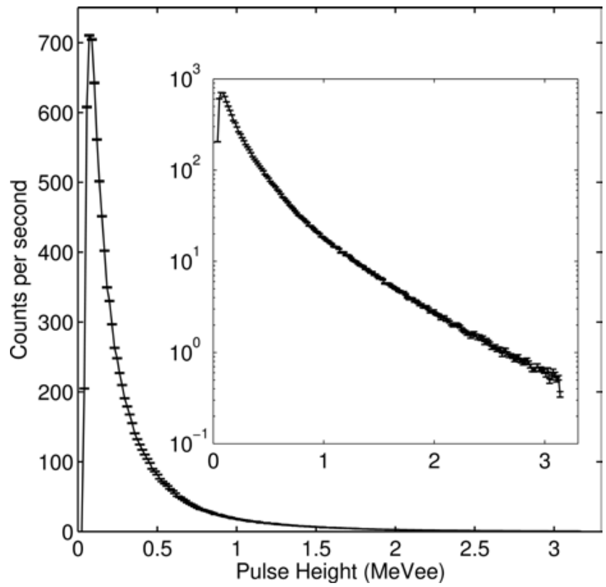

Fig. 4. Measured ^{252}Cf neutron pulse height distribution. Error bars shown are based on counting statistics and correspond to one standard deviation. The inset shows the same data on a semi-log scale. The detector size is 12.7 cm thick x 12.7 cm diameter.

5.0 MCNPX-PoliMi Simulation and MPPost Post-Processing: Results for 12.7 cm x 12.7 cm Detector

A simplified model of the detector was created in MCNPX-PoliMi. PoliMi's built-in ^{252}Cf sourcewas used, and energy depositing events were recorded in the cylindrical detector cell. MCNPX-PoliMi outputs a data file that tracks particle collisions, allowing the proper nonlinear light output to be generated due to multiple neutron events in the same history. For example, in the 12.7 cm x 12.7 cm detector, 68% of simulated neutron events had at least two hydrogen scatters in the first three interactions. These data highlight the importance of treating the nonlinear light output correctly.

An enhanced version of MPPost was used to post-process the data files and generate PHDs. The modifications allowed the use of the Birks and Voltz light output equations in addition to the pre-existing polynomial, rational, and exponential forms. Gaussian resolution broadening was applied using the following relationship

$$\frac{\Delta E}{E} = \sqrt{\alpha^2 + \frac{\beta^2}{E} + \left(\frac{\gamma}{E}\right)^2} \qquad (7)$$

with $\alpha = 0.102$, $\beta = 0.102$, and $\gamma = 0.036$ [13].

Fig.5showsthe fractional errorof simulated PHDs using the light output relationships in Table 2 as compared to measured data. Substantial variation in simulated PHDs occurs when the different fits are employed. In order to enhance the ability to determine the best agreement between simulated and measured PHDs, fractional difference plots were generated. These plots show the quantity $(S\text{-}M)/M$ in each bin, where S is the simulated number of counts and M is the measured number of counts.

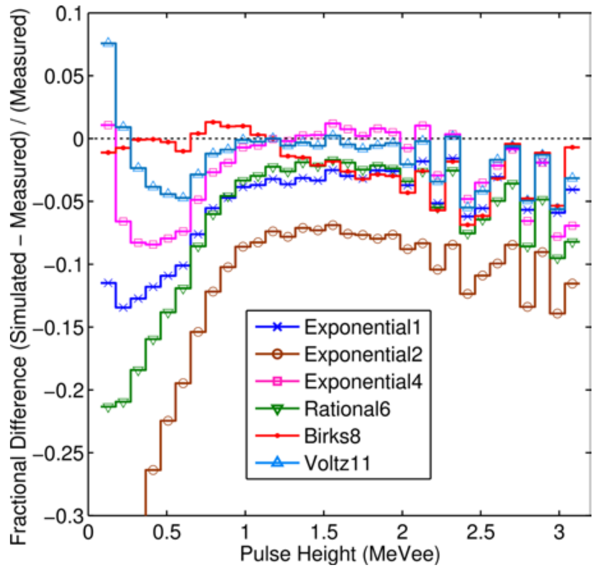

Fig.5. Fractional errorof simulated pulse height distributions for a selection of the tested light output functions. The best overall results were obtained using Birks8.

The exponentialfunctional form with d equal to1.05 (Exponential4) results in the best agreementofthe tested exponential models, but still has a tendency to under-predict the count rate at lower pulse heights. Birks8 performs the best over the full range of energies and pulse heights considered here. Using Birks8, we achieved better than 5% bin-by-bin agreement between simulated and measured PHDs over the range 0.08 to 2.18 MeVee, and better than 10% bin-by-bin agreement between 2.18 and 3.13 MeVee.

The simulated pulse height distribution with Exponential2 (d equal to 0.9) significantly under-predicts the measured pulse height distribution over the full range. These results demonstrate that the low-energy behavior of the light output fit affects the whole pulse height distribution, even when the fit and the $L(E)$ data points agree well in their energy range. The Exponential2 model has a rapid dropoff in light output below the fitted range, which results in two main effects: an increased minimum neutron energy deposition to exceed the threshold, and, importantly, a reduction in the total light produced for many neutron pulses due to multiple scatter events. The reduction in light from the secondary scatters in multiple scatter events accounts for the underprediction of the simulation at pulse heights higher than ~1 MeVee, even though the fit in Fig. 2 agrees well in that range.

We also compared the simulated total counts from 0.08to 3.13 MeVee to the experimental data. The results are presented in Table 3. The total counts agree within 1% using the Birks8 model, while the previous Exponential1 model differs by 11%. Below 0.08 MeVee, the simulated PHD exceeds the measured PHD due to particle misclassification in the measurement.

Table 3. Comparison of simulated (ΣS) and measured (ΣM) total counts from 0.08 to 3.13 MeVee for the 12.7 cm x 12.7 cm detector.

Model	$\frac{\Sigma S - \Sigma M}{\Sigma M}$
Exponential1	-11.0%
Exponential2	-33.6%
Exponential4	-3.5%
Rational6	-17.4%
Birks8	-0.7%

Voltz11	+1.8%

Fig.6 reprises Fig.2 but addsdata from the classic reference for neutron light output on protons, carbon, and alphas, Verbinskiand colleagues[31], and expands the high-energy extrapolationto 50 MeV. The Birks fit (Birks8) can be seen at higher energies to approach and then exceed the line L(E)=E, which is not physical. The best Voltz fit (Voltz11) and the best exponential fit (Exponential4) both behave more plausibly in the high energy extrapolation. In order to explore that region more fully, a similar experiment and simulation validation would need to be conducted at high energies.

There are significant differences between the detectors and measurement techniques used in this work and the ones from Verbinksi's, so the Verbinski data are not expected to perfectly agree with our data. However, it can be seen that these fits follow the general S-shape of the Verbinski data on log-log axes. This shape is inferred to be characteristic of proton light output in organic scintillators. The proton stopping power in EJ-309 liquid scintillator reaches a peak at 0.07 MeV. Below 0.07 MeV, the stopping power and thus quenching, is reduced, so the maximum quenching occurs near 0.07 MeV, causing an inflection point in the light output. In the case of Birks and Voltz, the stopping power is used directly, so this effect is captured. In the case of the exponential, this reduction in very low energy quenching could explain the better agreement achieved by setting the exponent *d* greater than 1.

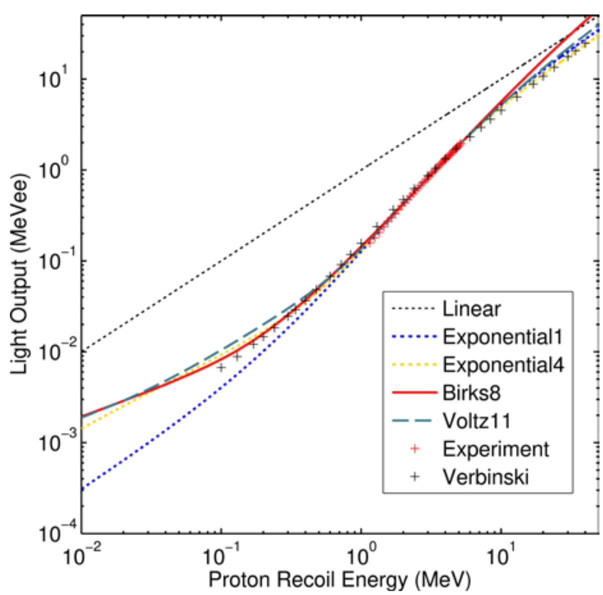

Fig.6. Log-log plot showing the measured light output data points for the 12.7 cm thick by 12.7 cm diameter EJ-309 detector as well as the various fits extrapolated from 0.01 to 7 MeV proton recoil energy. Additionally, the NE-213 neutron light output data from Verbinski is shown. [31]

5.1 Results for 7.62 cm x 7.62 cm EJ-309 Detector

We also reexamined the neutron light output data from Enqvist and colleagues [13] for the 7.62 cm x 7.62 cm detector, but used an updated energy deposition calibration point. We used the following calibration method for all of the data presented in this work, but the effects of miscalibration are most clearly demonstrated by the 7.62 cm x 7.62 cm data, so we present it here.

We determined that the Cs-137 Compton edge calibration point used to generate the fit in [13] was 0.290 V, corresponding to 478 keVee. To check that calibration point, we used a method similar to that of [32]; we simulated an unbroadenedPHD due to Cs-137 gamma-ray interactions in the detector, applied varying resolution functions, and scaled and matched the measured PHD to the simulation to determine the appropriate calibration point.

Fig. 7 shows the new calibration point determined using this method. The black dotted line shows the simulated pulse height distribution due to Cs-137, with no resolution broadening applied. The Compton edge is located at the straight vertical line. After applying resolution broadening, the fractional edge of the broadened peak corresponding to the Compton edge could be determined by finding the intersection of the vertical line and the broadened distribution. This fractional edge value was then applied to the measured pulse height distribution, and the distributions scaled to match the peak heights. This process was iterated over a variety of resolution functions and the best agreement was chosen by visual inspection; in future work an automated test of agreement can be used.A resolution function with a value of 15% at 478 keV resulted in a fractional edge of 83% and a calibration point of 0.3065 V.

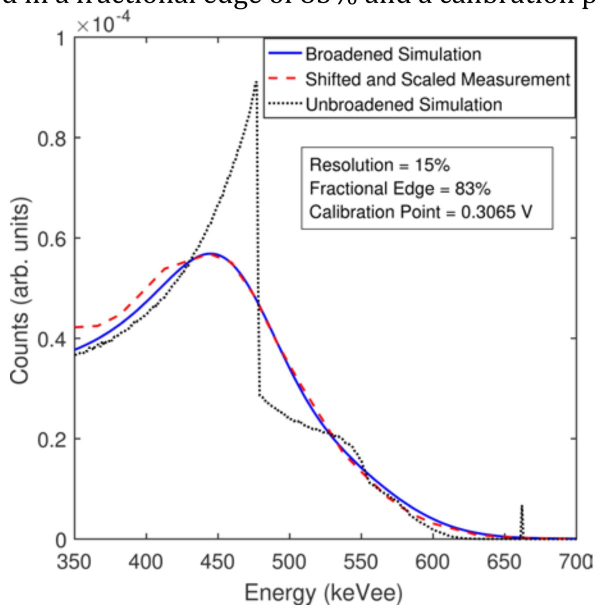

Fig. 7. The calibration point for the 7.62 cm x 7.62 cm EJ-309 detector used in the *L(E)* measurement. The black dotted line shows the simulated pulse height distribution due to Cs-137 662 keV gamma rays in the detector, without resolution broadening. The solid blue line and dashed red line show the broadened simulation and calibrated measured pulse height distributions.

The new calibration point resulted in a reduction of 5.7% of the light output for each energy-light output pair compared to [13]. The new light output data points were fitted to the exponential, Birks, and Voltz models. The coefficients for the resultant fits are listed in Table 4. The fractional differences between the validation measurement of ^{252}Cf neutrons and the simulated PHD are shown in Fig. 8. The agreement using any of these fits is a significant improvement over the function in [13] (Exponential1). The integrated counts from 0.09 to 3.2 MeVee agreed to within 3.5% using Birks8, 2% using Voltz11, and within less than 1% using Exponential2 (d = 1.05), while the previous exponential fit, Exponential1, differed by 13%. The fractional difference curves of Fig. 8are not as “flat” as the ones shown in Fig. 5 for the 12.7 cmby 12.7 cm detector. The slight remaining slope in Fig. 8 could be due to detector-specific variation (the detector used for the validation was the same type as the one used to measure the light output, but not the identical detector) or to an unknown systematic error in the original experimental data.

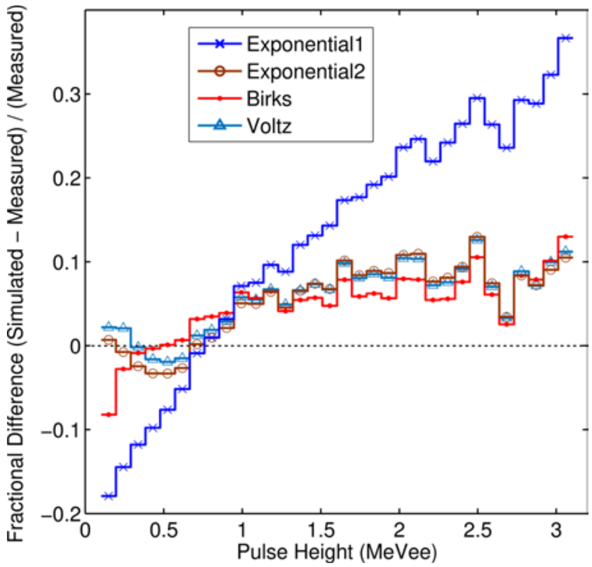

Fig. 8. Fractional errorof simulated pulse height distributions for a selection of the tested light output functions. The detector size is 7.62 cm thick x 7.62 cm diameter.

Table 4. Light output model coefficients for the 7.62 cm thick x 7.62 cm diameter EJ-309 detector. Italics indicate coefficients that were fixed during the fitting process.

Form	a	b	c	d	SSE	R^2	RMSE	ID
Exponential	*0.817*	*2.63*	*0.297*	*1.000*	0.1694	0.9694	0.0764	Exponential1*
	0.668	1.63	0.387	*1.050*	0.0040	0.9993	0.0121	Exponential2
Birks	1.903	26.03			0.0043	0.9992	0.0124	Birks
Voltz	*1*	8.447	0.1072		0.0039	0.9993	0.0183	Voltz

*Fit from [13].

Table 5. Comparison of simulated (ΣS) and measured (ΣM) total counts from 0.08 to 3.13 MeVee for the 7.62 cm x 7.62 cm detector.

Model	$\frac{\Sigma S - \Sigma M}{\Sigma M}$
Exponential1	-11.7%
Exponential2	-0.2%
Birks	-3.3%
Voltz	+1.6%

6.0 Discussion

It is necessary to use a light output model that is robust in extrapolation to low energies. Typically, accurate light output measurements at low energies become difficult due to accelerator, source, or geometric constraints, imposing an effective threshold. Creative experiment design can alleviate some of these issues, and indeed there is a need for robust measurement of the light output from neutrons depositing low amounts of energy. In any event, if one chooses a model that is physics-based and realistic, one can be more confident in extrapolation to energies below the measured light output data points.

We performed a comprehensive study of a variety of possible scintillator light output models. Our results add to thebody of worksupporting the theory that light output quenching is proportional to stopping power. Both of the semi-empiricalmodels we tested account for this effect.

The stopping power data arereadily available in the SRIM package. Once the initial integration functionsare established, the semi-empirical forms are not difficult to use. The lookup table of L(E) that is generated can be used in both directions.

An advantage of the semi-empirical forms is that some of the coefficients are material dependent, while others are expected to be detector and calibration dependent. It may be the case that the same parameterization can be used for multiple detectors of the same type, and it may further be possible to adjust for detector-to-detector variations in a logical way by adjusting only thedetector-dependent parameters.

The determination of the MeVee/MeV calibration scale is of great importance in this type of work. A difference as small as 0.01V in the identified Compton edge location can significantly change the "steepness" of the light output curve, affecting the fitted coefficients and in turn the simulated PHDsand other derived parameters. The best effort to calibrate to the true Compton edge,accounting for detector resolution and multiple scatters, must be made. Uncertainties in this area can be mitigatedby ensuring that the calibration method used for the generation of the light output curve is the same as that used for the validation measurement, but it is clearly preferable that the calibration point be as close as possible to the "true" Compton edge pulse height.

We suspect that some difficulties previously encountered with neutron unfolding on the basis of simulated response matrices may be ameliorated by the use of more accurate light output models. The light output changes the effective thresholds and strongly influences energy-dependent efficiency, which is a key parameter in unfolding algorithms.

In general, researchers should make every effort to obtain the best possible light output data for their specific detectors, generate fits using the semi-empirical forms, and test their results using a Monte Carlo code such as MCNPX-PoliMi (available through RSICC). If measuring the light output directly is not an option, caution must be utilized when applying light output functions and coefficients generated by other researchers—even a small difference in calibration or measurement technique can cause significant deviations. While the entire process is highly sensitive, we have shown that if great care is taken, excellent agreement between simulation and measurement can be obtained.

7.0 Summary and Conclusions

The neutron light output data of Enqvistand colleagues[13]were analyzed with a variety of light output equations. The extrapolations of these equationswere shown to diverge widely, especially at low energy. A measurement of neutrons from a ^{252}Cfsource and simulation of the same were validated against each other, utilizing the various equations. The best equationsresulted in the best agreement between simulation and measurement. We achieved better than 5% bin-by-bin agreement between simulated and measured PHDs over the range 0.08 to 2.18 MeVee, and better than 10% agreement between 2.18 and 3.13 MeVee. The integrated counts from above 0.08 MeVee agree within 1% using the Birks8 model, while the previous Exponential1 model differed by 11%. Below 0.08 MeVee, the simulated PHD exceeds the measured PHD due to particle misclassification in the measurement.

We have demonstrated that the choice of model to represent theneutron light output from organic scintillators as a function of energy deposited is a critical step in detector characterization. A wide variety of modelscan be chosen from the literature, and most allow good fits to measured light output data. It is not possible, therefore, to select among them only on the basis of fit quality. A good fit to the data is necessary, but not sufficient.

Extrapolation to lower energies is particularly sensitive to the functional form used. Low-energy collisions cannot be neglected because neutrons can undergo multiple scatters in organic scintillators; multiple sub-threshold scatters can generate an amount of light that exceeds the threshold, and sub-threshold scatters can be present in larger pulses as well. The summation is nonlinear and the result depends strongly on the light output model used.

Therefore, the use of a detector response code to thoroughly test the selected model and fitted coefficients is beneficial. MCNPX-PoliMi and MPPost have been shown to beeffective codes for this purpose, in conjunction with validation experiments using a neutron source with a well-known energy spectrum and emission rate, such as a recently-calibrated ^{252}Cf spontaneous fission source.

The semi-empirical light output equations proposed by Birks and Voltz are grounded in theoryand make use of stopping power data to model quenching. The stopping power dependence enables fitting of coefficients at light outputs where the data are easier to obtain and/or more reliable and guides extrapolation to low energies with greater confidence than that provided by the more arbitrary parameterizations. We have shown that the Birks model works particularly well for EJ-309 liquid scintillation detectors of two different sizes (right cylindrical cells, 12.7 cm x 12.7 cm and 7.62 cm x 762 cm), and achieved excellent agreement between our simulated and measured ^{252}Cf neutron pulse height distributions.

Acknowledgments

This research was performed under appointment to the Nuclear Nonproliferation International Safeguards Fellowship Program sponsored by the National Nuclear Security Administration's Office of International Nuclear Safeguards (NA-241).
This work was funded in-part by the Consortium for Verification Technology under Department of Energy National Nuclear Security Administration award number DE-NA0002534.

References

[1] D. Henzlova, R. Kouzes, R. McElroy, P. Peerani, M. Aspinall, K. Baird, A. Bakel, M. Borella, M. Bourne, L. Bourva, F. Cave, R. Chandra, D. Chernikova, S. Croft, G. Dermody, A. Dougan, J. Ely, E. Fanchini, P. Finocchiaro, V. Gavron, M. Kureta, K.D. Ianakiev, K. Ishiyama, T. Lee, C. Martin, K. McKinny, H.O. Menlove, C. Orton, A. Pappalardo, B. Pedersen, D. Peranteau, R. Plenteda, S. Pozzi, M. Schear, M. Seya, E. Siciliano, S. Stave, L. Sun, M.T. Swinhoe, H. Tagziria, S. Vaccaro, J. Takamine, A.-L. Weber, T. Yamaguchi, H. Zhu, Current Status of Helium-3 Alternative Technologies for Nuclear Safeguards, Los Alamos, NM (United States), 2015. doi:10.2172/1227248.

[2] J.L. Dolan, M. Flaska, A. Poitrasson-Riviere, A. Enqvist, P. Peerani, D.L. Chichester, S.A. Pozzi, Plutonium measurements with a fast-neutron multiplicity counter for nuclear safeguards applications, Nucl. Instruments Methods Phys. Res. Sect. A Accel. Spectrometers, Detect. Assoc. Equip. 763 (2014) 565–574. doi:10.1016/j.nima.2014.06.028.

[3] D.L. Chichester, S.J. Thompson, M.T. Kinlaw, J.T. Johnson, J.L. Dolan, M. Flaska, S.A. Pozzi, Statistical estimation of the performance of a fast-neutron multiplicity system for nuclear material accountancy, Nucl. Instruments Methods Phys. Res. Sect. A Accel. Spectrometers, Detect. Assoc. Equip. 784 (2015) 448–454. doi:10.1016/j.nima.2014.09.027.

[4] M.G. Paff, M.L. Ruch, A. Poitrasson-Riviere, A. Sagadevan, S.D. Clarke, S. Pozzi, Organic liquid scintillation detectors for on-the-fly neutron/gamma alarming and radionuclide identification in a pedestrian radiation portal monitor, Nucl. Instruments Methods Phys. Res. Sect. A Accel. Spectrometers, Detect. Assoc. Equip. 789 (2015) 16–27. doi:10.1016/j.nima.2015.03.088.

[5] M.G. Paff, S.D. Clarke, S.A. Pozzi, Organic liquid scintillation detector shape and volume impact on radiation portal monitors, Nucl. Instruments Methods Phys. Res. Sect. A Accel. Spectrometers, Detect. Assoc. Equip. 825 (2016) 31–39. doi:10.1016/j.nima.2016.03.102.

[6] A. Poitrasson-Rivière, J.K. Polack, M.C. Hamel, D.D. Klemm, K. Ito, A.T. McSpaden, M. Flaska, S.D. Clarke, S.A. Pozzi, A. Tomanin, P. Peerani, Angular-resolution and material-characterization measurements for a dual-particle imaging system with mixed-oxide fuel, Nucl. Instruments Methods Phys. Res. Sect. A Accel. Spectrometers, Detect. Assoc. Equip. 797 (2015) 278–284. doi:10.1016/j.nima.2015.06.045.

[7] A. Poitrasson-Rivière, M.C. Hamel, J.K. Polack, M. Flaska, S.D. Clarke, S.A. Pozzi, Dual-particle imaging system based on simultaneous detection of photon and neutron collision events, Nucl. Instruments Methods Phys. Res. Sect. A Accel. Spectrometers, Detect. Assoc. Equip. 760 (2014) 40–45. doi:10.1016/j.nima.2014.05.056.

[8] A. Poitrasson-Rivière, B. a. Maestas, M.C. Hamel, S.D. Clarke, M. Flaska, S.A. Pozzi, G. Pausch, C.-M. Herbach, A. Gueorguiev, M.F. Ohmes, J. Stein, Monte Carlo investigation of a high-efficiency, two-plane Compton camera for long-range localization of radioactive materials, Prog. Nucl. Energy. 81 (2015) 127–133. doi:10.1016/j.pnucene.2015.01.009.

[9] S. Yoshida, T. Ebihara, T. Yano, a. Kozlov, T. Kishimoto, I. Ogawa, R. Hazama, S. Umehara, K. Mukaida, K. Ichihara, Y. Hirano, I. Murata, J. Datemichi, H. Sugimoto, Light output response of KamLAND liquid scintillator for protons and 12C nuclei, Nucl. Instruments Methods Phys. Res. Sect. A Accel. Spectrometers, Detect. Assoc. Equip. 622 (2010) 574–582. doi:10.1016/j.nima.2010.07.087.

[10] S.A. Pozzi, M.M. Bourne, J.L. Dolan, K. Polack, C. Lawrence, M. Flaska, S.D. Clarke, A. Tomanin, P. Peerani, Plutonium metal vs. oxide determination with the pulse-shape-discrimination-capable plastic scintillator EJ-299-33, Nucl. Instruments Methods Phys. Res. Sect. A Accel. Spectrometers, Detect. Assoc. Equip. 767 (2014) 1–5. doi:10.1016/j.nima.2014.08.002.

[11] S.D. Clarke, B.M. Wieger, E. Pryser, R. Arghal, S.A. Pozzi, R.A. Halg, V.A. Bashkirov, R.W. Schulte, Characterization of secondary neutron production during proton therapy, in: 2014 IEEE Nucl. Sci. Symp. Med. Imaging Conf., IEEE, 2014: pp. 1–3. doi:10.1109/NSSMIC.2014.7431166.

[12] S.D. Clarke, M.A. Norsworthy, E. Pryser, S.A. Pozzi, R.A. Halg, V.A. Bashkirov, R.W. Schulte, M. Pankuch, Measurement of neutrons and photons produced during proton therapy, in: 2015 IEEE Nucl. Sci. Symp. Med. Imaging Conf., IEEE, 2015.

[13] A. Enqvist, C.C. Lawrence, B.M. Wieger, S.A. Pozzi, T.N. Massey, Neutron light output response and resolution functions in EJ-309 liquid scintillation detectors, Nucl. Instruments Methods Phys. Res. Sect. A Accel. Spectrometers, Detect. Assoc. Equip. 715 (2013) 79–86. doi:10.1016/j.nima.2013.03.032.

[14] R.C. Byrd, W.T. Urban, LA-12833-MS: Calculations of the Neutron Response of Boron-Loaded Scintillators, 1994.

[15] R.J. Kurz, UCRL-11339: A 709/7090 Fortran II Program to Compute the Neutron-Detection Efficiency of Plastic Scintillator for Neutron Energies from 1 to 300 MeV, Berkeley, CA, 1964.

[16] J.B. Birks, The Theory and Practice of Scintillation Counting, Pergamon Press Ltd., 1964.

[17] F.D. Brooks, Development of organic scintillators, Nucl. Instruments Methods. 162 (1979) 477–505. doi:10.1016/0029-554X(79)90729-8.

[18] R. Voltz, J. Lopes da Silva, G. Laustriat, A. Coche, Influence of the Nature of Ionizing Particles on the Specific Luminescence of Organic Scintillators, J. Chem. Phys. 45 (1966) 3306 – 3311. doi:10.1063/1.1728106.

[19] S.P. Ahlen, B.G. Cartwright, G. Tarlé, Return to unsaturated response of polymeric scintillators excited by relativistic heavy ions, Nucl. Instruments Methods. 147 (1977) 321–328. doi:10.1016/0029-554X(77)90264-6.

[20] S.A. Pozzi, S.D. Clarke, W.J. Walsh, E.C. Miller, J.L. Dolan, M. Flaska, B.M. Wieger, A. Enqvist, E.

Padovani, J.K. Mattingly, D.L. Chichester, P. Peerani, MCNPX-PoliMi for nuclear nonproliferation applications, Nucl. Instruments Methods Phys. Res. Sect. A Accel. Spectrometers, Detect. Assoc. Equip. 694 (2012) 119–125. doi:10.1016/j.nima.2012.07.040.

[21] E.C. Miller, S.D. Clarke, M. Flaska, S.A. Pozzi, E. Padovani, MCNPX-PoliMi Post-processing Algorithm for Detector Response Simulations, J. Nucl. Mater. Manag. 40 (2012).

[22] N. V. Kornilov, I. Fabry, S. Oberstedt, F.J. Hambsch, Total characterization of neutron detectors with a 252Cf source and a new light output determination, Nucl. Instruments Methods Phys. Res. Sect. A Accel. Spectrometers, Detect. Assoc. Equip. 599 (2009) 226–233. doi:10.1016/j.nima.2008.10.032.

[23] J.F. Ziegler, SRIM-2013, (2013). srim.org.

[24] J.F. Ziegler, J.P. Biersack, M.D. Ziegler, SRIM: The Stopping and Range of Ions in Matter, 15th Ed., 2015.

[25] NIST, ESTAR: Stopping-power and Range Tables for Electrons, (2015). physics.nist.gov/PhysRefData/Star/Text/ESTAR.html.

[26] MATLAB and Curve Fitting Toolbox Release 2016a, The MathWorks, Inc., Natick, Massachusetts, United States, (2016).

[27] M. Takada, K. Yajima, S. Kamada, Simulated Neutron Response Functions of Phoswich-Type Neutron Detector and Thin Organic Liquid Scintillator, Aesj.or.Jp. 2 (2011) 274–279. http://www.aesj.or.jp/publication/pnst002/data/274-279.pdf.

[28] R. Madey, F.M. Waterman, A.R. Baldwin, J.N. Knudson, J.D. Carlson, J. Rapaport, The response of NE-228A, NE-228, NE-224, and NE-102 scintillators to protons from 2.43 to 19.55 MeV, Nucl. Instruments Methods. 151 (1978) 445–450. doi:10.1016/0029-554X(78)90154-4.

[29] L.F. Miller, J. Preston, S. Pozzi, M. Flaska, J. Neal, Digital pulse shape discrimination, Radiat. Prot. Dosimetry. 126 (2007) 253–255. doi:10.1093/rpd/ncm052.

[30] J.K. Polack, M. Flaska, A. Enqvist, C.S. Sosa, C.C. Lawrence, S.A. Pozzi, An algorithm for charge-integration, pulse-shape discrimination and estimation of neutron/photon misclassification in organic scintillators, Nucl. Instruments Methods Phys. Res. Sect. A Accel. Spectrometers, Detect. Assoc. Equip. 795 (2015) 253–267. doi:10.1016/j.nima.2015.05.048.

[31] V.V. Verbinski, W.R. Burrus, T. A. Love, W. Zobel, N.W. Hill, R. Textor, Calibration of an organic scintillator for neutron spectrometry, Nucl. Instruments Methods. 65 (1968) 8–25. doi:10.1016/0029-554X(68)90003-7.

[32] G. Dietze, H. Klein, Gamma-calibration of NE 213 scintillation counters, Nucl. Instruments Methods. 193 (1982) 549–556. doi:10.1016/0029-554X(82)90249-X.